Available online at www.sciencedirect.com
ScienceDirect
Ceramics International 35 (2009) 1709–1718
CERAMICS INTERNATIONAL
www.elsevier.com/locate/ceramint

Oxidation modeling of a Si_3N_4–TiN composite: Comparison between experiment and kinetic models

F. Deschaux-Beaume [a,*], N. Frety [b], T. Cutard [c], C. Colin [d]

[a] Université de Montpellier 2, LMGC, 34095 Montpellier, France
[b] Université de Montpellier 2, LPMC, 34095 Montpellier, France
[c] Université de Toulouse, Mines Albi, CROMeP, Campus Jarlard, 81013 Albi Cedex 09, France
[d] Ecole des Mines de Paris, Centre des Matériaux, 91000 Evry, France

Received 29 May 2008; received in revised form 15 July 2008; accepted 18 September 2008
Available online 1 October 2008

Abstract

Based on microstructural observations, a phenomenological oxidation model and associated oxidation kinetics have been developed for a Si_3N_4–50 wt.%TiN ceramic composite. Above 1000 °C, the oxidation mechanism is complex and has been described in a three-step model. In a first step, the oxidation of TiN in TiO_2 is controlled by titanium diffusion, whereas Si_3N_4 oxidation in SiO_2 is controlled by O diffusion through SiO_2. The outward diffusion of Ti creates pores in the sub-layer, which decrease the Ti migration rate. In a second step, the oxidation is controlled by oxygen diffusion, both through SiO_2 and TiO_2, and SiO_2 progressively fills the porosity due to the outward diffusion of Ti. In the third step, SiO_2 covers the sub-layer entirely, and the oxidation is controlled by O diffusion through SiO_2.

Isothermal and non-isothermal thermogravimetric analyses (TGA) have been carried out on the Si_3N_4–TiN composite under air up to 1200 °C, in order to compare experimental data with the three-step oxidation model. An analysis method for non-isothermal TGA is presented. The results of this analysis, and of isothermal TGA, have enabled the identification of the main kinetic parameters characterizing the three steps of the oxidation kinetic model. The kinetic models corresponding to the first two oxidation step are in proper accordance with the experiment, whereas a gap is observed between the parabolic kinetic model of the third step and the experiment.

Keywords: B. Composites; C. Diffusion; D. Silicon nitride; D. Nitrides

1. Introduction

Si_3N_4–TiN ceramic composites are attractive materials, because they combine the good mechanical properties at high temperature of Si_3N_4 based ceramics with the ability to electro-discharge machining (EDM) [1–3]. However, these materials have the disadvantage of being more oxidation sensitive than pure Si_3N_4 ceramic. This phenomenon is primarily due to the presence of a continuous TiN network, which facilitates the inner oxidation of the TiN phase.

Due to the multiphasic character of the material, the oxidation process is very complex. While the phenomenon is not actually completely understood, some studies have shown that oxidation of Si_3N_4–TiN composites is diffusion-controlled [4–7]. Nevertheless, oxidation kinetics is generally complex and depends greatly on oxidation conditions and material composition.

Oxidation of pure silicon nitride starts above 1000 °C and leads to the formation of a SiO_2 amorphous layer on the surface, separated from the core material by a thin layer of a graded suboxide (SiN_xO_y) [8–10] or a crystalline oxynitride (Si_2N_2O) [11–17]. Oxidation is then controlled by the diffusion of oxygen through the SiO_2 and oxynitride layers. Sintered silicon nitride generally oxidises more quickly than pure silicon nitride [18–23]. This is related to the presence of an intergranular phase originating from sintering additives (Y_2O_3 and Al_2O_3). Some species (Y, Al and O) are more mobile in this phase than in Si_3N_4 at high temperature. Oxidation is then the result of the inward diffusion of oxygen through the oxide layer and the outward diffusion of yttrium

* Corresponding author. Tel.: +33 4 66 62 85 86 fax: +33 4 66 62 85 31.
E-mail address: deschaux@iut-nimes.fr (F. Deschaux-Beaume).

0272-8842/$34.00
doi:10.1016/j.ceramint.2008.09.006

and aluminum species through the intergranular phase. Oxidation kinetics, therefore, depends on the composition and amount of the intergranular phase [20].

The oxidation of titanium nitride to rutile (TiO_2) starts at a lower temperature than Si_3N_4, between 500 and 600 °C. It is observed that the oxidation is controlled via oxygen diffusion through TiO_2 especially at temperatures <1000 °C [6,24–26]. At higher temperatures, the rate-controlling mechanism is not clearly identified but a cationic diffusion of titanium may be supposed with the outward growth of rutile crystals and the observed porosity under the rutile layer [27,28].

On the basis of this data from the literature, and on microstructural investigations, an oxidation model has previously been proposed, for a Si_3N_4–TiN ceramic composite containing 30 vol.% of TiN [29]. Based on a phenomenological approach, the oxidation process has been described as a 3-step sequence of elementary mechanisms. Kinetic equations have been associated to each elementary mechanism in a previous article [30], in order to develop a global kinetic model for the oxidation of a Si_3N_4–TiN material. In this paper, an experimental study of oxidation kinetics, based on thermogravimetric analyses, has been carried out. The validity of the kinetic model presented is then discussed by comparison with this experimental data.

2. Experimental details

2.1. Material

A commercial composite (Kersit 601, Norton Desmarquest, FR), consisting in Si_3N_4 and TiN in equivalent weight proportions, was used for this study. The ceramic microstructure (Fig. 1) consists in TiN grains, surrounded by a Si_3N_4 based matrix, containing a fine SiYAlON intergranular phase formed from sintering additives (Y_2O_3 and Al_2O_3). The size distribution and the proportion of TiN particles in the material (50 wt.%, i.e. 30 vol.%) have been chosen to form a continuous TiN network, conferring on the material a sufficient electrical conductivity for EDM, without significant decrease in mechanical characteristics [2]. The microstructure of the as-received and oxidized material was characterized by scanning electron microscopy (SEM), and by energy dispersive spectrometry (EDS).

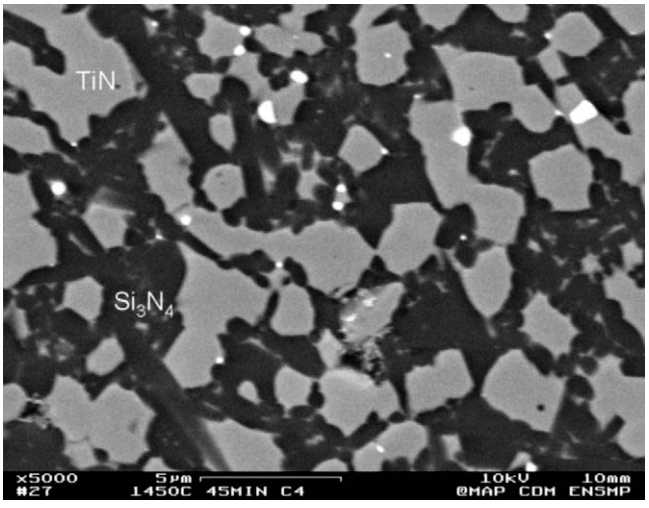

Fig. 1. Microstructure of the silicon nitride–titanium nitride ceramic.

2.2. Thermogravimetric analysis (TGA)

Thermogravimetric measurements were carried out under dynamic sweeping air (80 vol.%N_2–20 vol.%O_2) in a SETARAM TGA 24 apparatus. Ceramic samples, with a parallelepiped geometry ($22.5 \times 7.5 \times 1.5\ mm^3$), were machined by EDM process and finished with diamond tools.

Two types of test were carried out:

- *Isothermal tests, in the 800–1200 °C temperature range*. A high heating rate of 100 °C/min was chosen for these tests, in order to limit the non-isothermal oxidation before holding the temperature. The dwell time is 108 h for each test.
- *Non-isothermal tests, at constant heating rate from room temperature up to 1200 °C*. Six different heating rates were chosen for these tests: 0.5, 1, 3, 5, 10 and 20 °C/min. The main advantage of these non-isothermal tests is their short duration (1–40 h depending on the heating rate, against 108 h for isothermal tests). They have been used to determine with accuracy the kinetic parameters corresponding to the oxidation at low temperature, which is important data for modeling the oxidation steps in the proposed model. An original analysis method for these tests was developed, and is detailed in the following section.

2.3. Analysis method for non-isothermal TGA data

The analysis method for non-isothermal TGA is based on time–temperature equivalence relation of thermally activated processes. For a given thermally activated mechanism occurring between temperatures T_1 and T_2, the quantity affected by the phenomenon at a temperature T_2 after a time t_2, is the same as at a temperature T_1 after a time t_1, if relation (1) is verified [31,32]:

$$\frac{t_1}{t_2} = \exp\left(-\frac{E_a}{R}\left(\frac{1}{T_2} - \frac{1}{T_1}\right)\right) \quad (1)$$

where E_a is the activation energy of the mechanism, and R is the gas constant.

Considering that a heating ramp between the temperature T_0 and T_M at a constant heating rate λ is equivalent to the succession of isothermal dwell of duration dt (Fig. 2), relation (1) can be applied to each ramp increment, if the considered phenomenon is controlled by the same mechanism between T_0 and T_M. Each ramp increment of duration dt and temperature T ($T_0 \le T \le T_M$) can then be associated to an equivalent increment at temperature T_M of duration dt_e, verifying Eq. (2) (Fig. 2):

$$\frac{dt_e}{dt} = \exp\left(-\frac{E_a}{R}\left(\frac{1}{T} - \frac{1}{T_M}\right)\right) \quad (2)$$

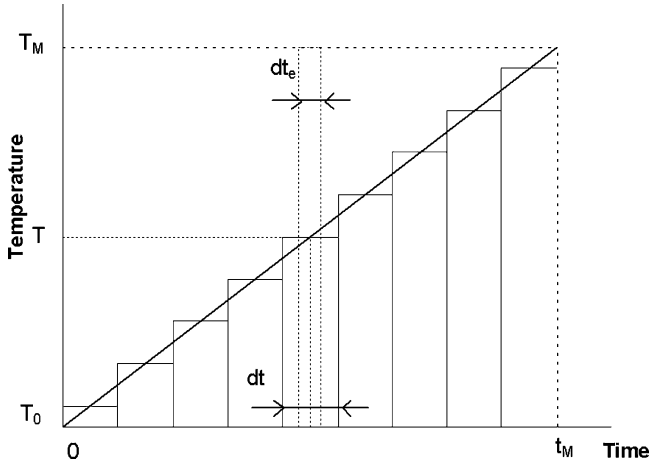

Fig. 2. Analysis method for non-isothermal TGA.

Integrating this relation on the whole of the ramp duration, from $t = 0$ to $t = t_M$, the equivalent time, t_e, giving the same affected quantity during an isothermal dwell at temperature T_M as during a heating ramp between T_0 and T_M, at the heating rate λ, can then be expressed according to the following equation:

$$t_e = \int_0^{t_M} \exp\left(-\frac{E_a}{R}\left(\frac{1}{T} - \frac{1}{T_M}\right)\right) dt \quad (3)$$

where

$$T = T_0 + \lambda t$$

with

$$\lambda = \frac{T_M - T_0}{t_M}$$

This integral has been previously calculated by Toitot and Dor [32] using a variable change:

$$t_e = -\frac{RT_M^2}{E_a \lambda}\left(\exp\left(-\frac{E_a}{RT_M}\frac{T_M - T_0}{T_M}\right) - 1\right) \quad (4.a)$$

According to Toitot and Dor [32], when $T_M \gg T_0$, the t_e value can be expressed as

$$t_e \approx \frac{RT_M^2}{E_a}\frac{1}{\lambda} \quad (4.b)$$

If the considered phenomenon is an oxidation mechanism controlled by diffusion, then the mass gain per unit area, $\Delta m/S$, during the heating ramp is given by relation (5):

$$\frac{\Delta m}{S} = k_p^{1/2} t_e^{1/2} \quad (5)$$

where k_p is the parabolic rate constant of the oxidation process, at the maximal temperature of the ramp T_M:

$$k_p = k_0 \exp\left(-\frac{E_a}{RT_M}\right) \quad (6)$$

where k_0 is a proportionality constant.

Introducing expression (4.b) in relation (5), the equation can be transformed into the relation (7) [33,34]:

$$\ln\frac{\lambda^{1/2}}{T_M} = -\frac{E_a}{2R}\frac{1}{T_M} + \frac{1}{2}\ln\frac{k_0 R}{E_a(\Delta m/S)^2} \quad (7)$$

This relation is convenient as the $\ln(\lambda^{1/2}/T_M)$ function has a linear dependence with $1/T_M$ at a constant $\Delta m/S$ mass gain per unit area, if the heating ramp is carried out in a temperature range corresponding to a single diffusion mechanism. The proportionality factor of the $\ln(\lambda^{1/2}/T_M) = f(1/T_M)$ function is then proportional to the activation energy of the phenomenon. According to relation (7), it is then possible to determine the activation energy of the oxidation mechanism, from a set of non-isothermal TGA curves performed at different heating rates λ.

3. Experimental results

3.1. Microstructural analysis of oxidized samples

For the samples oxidized below 900 °C, only the superficial TiN particles were transformed into TiO_2, whereas the Si_3N_4 phase remains unoxidized (Fig. 3a).

In contrast, above 1000 °C, the surface of the samples is completely covered by TiO_2, revealing a Ti diffusion towards the surface (Fig. 3b). The cross-section of the oxidized samples at high temperature shows three successive layers (Fig. 4). The morphology of this oxidized area is similar to that observed by Gogotsi et al. [4,5] and by Bellosi et al. [6] on similar materials. The first layer (outer layer) is mainly composed of TiO_2 (rutile) crystals, as observed on the top view of the sample surface (Fig. 3b). The second layer (intermediate layer) is composed of isolated TiO_2 crystals, and a continuous SiO_2 phase presenting a glassy aspect. This second layer contains large spherical pores of 2 to 10 or 20 μm diameters. The third layer (inner layer) exhibits a more complex microstructure consisting of several phases and porosity. Microstructural gradients are observed both on SEM micrographs and on EDS results in this layer. Close to the interface with the second layer, the initial TiN grains have been replaced mainly by TiO_2 crystals, whereas in the center of the layer and close to the oxidation front, they have been replaced mainly by porosity, due to an outward diffusion of titanium. In contrast, the Si_3N_4 phase remains unoxidized in the inner oxidation layer.

3.2. Isothermal TGA curves

The transformation of silicon and titanium nitrides in oxides (with nitrogen release) takes place with a mass gain which can be measured by thermogravimetric investigations.

Fig. 5 shows the evolution of sample mass during isothermal oxidation tests performed at different temperatures between 800 and 1200 °C.

Below 900 °C, the oxidation kinetic can be modeled, after a transitory initial mode, by a parabolic law (Fig. 6):

$$\frac{\Delta m}{S} = K^{1/2} t^{1/2} + \frac{\Delta m_0}{S} \quad (8)$$

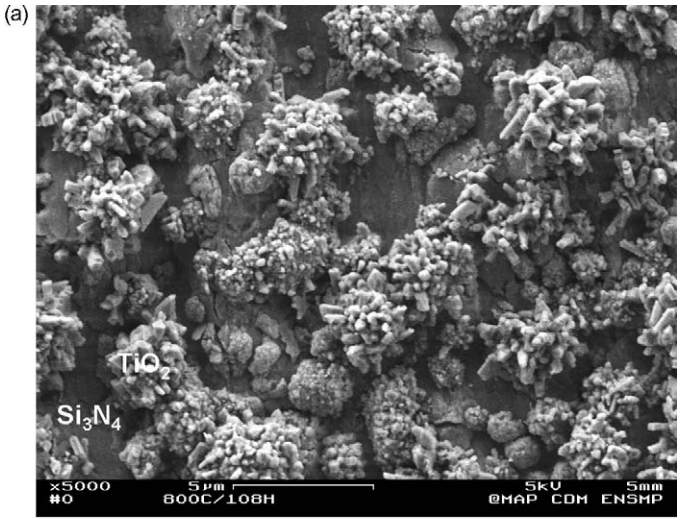

Fig. 3. Micrographs of the Si_3N_4–TiN surface after a 108 h oxidation treatment at 800 °C (a) and 1150 °C (b).

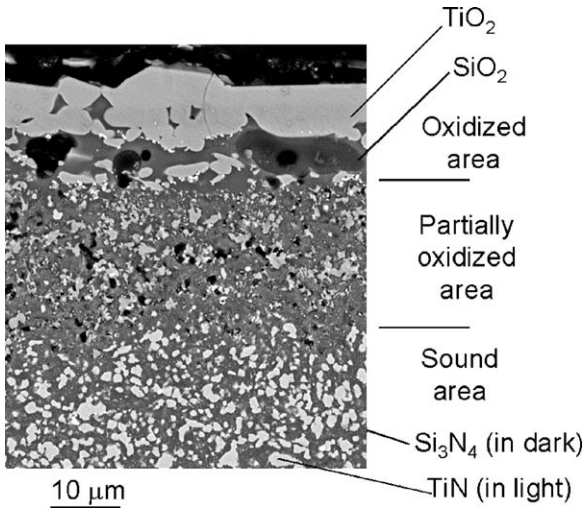

Fig. 4. Cross-section (SEM micrograph) of the Si_3N_4–TiN ceramic after a 100 h oxidation at 1150 °C.

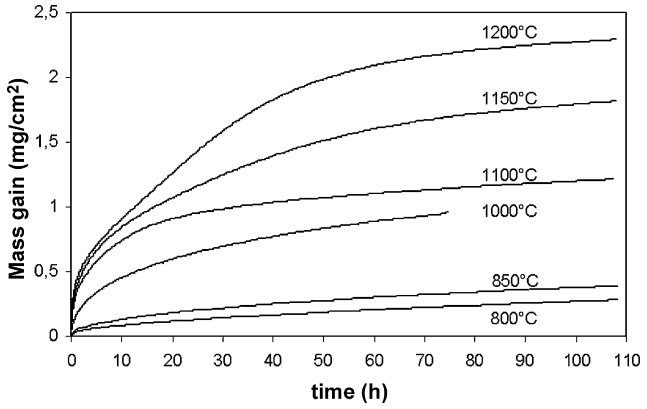

Fig. 5. Isothermal TGA curves showing the oxidation kinetic of the Si_3N_4–TiN ceramic in air between 800 and 1200 °C.

where Δm is the mass gain at the time t, Δm_0 is the mass gain at the beginning of the isothermal oxidation ($t = 0$), S is the surface exposed to oxidation, and K is a constant (apparent parabolic rate constant).

This oxidation mode, which corresponds to a diffusion-controlled mechanism, is compatible with the data resulting from the previously proposed model [29,30], and from the literature [4–7]. At low temperatures, only the TiN phase is oxidized and the process is controlled by the diffusion of oxygen through the formed TiO_2.

Above 1000 °C on the other hand, the oxidation kinetic is not perfectly parabolic. A retardation of the mass gain compared to the parabolic kinetic is then observed after a few oxidation hours (Fig. 6). This phenomenon shows the complexity of the oxidation process above 1000 °C. Several diffusional mechanisms then take place at the same time, and the oxidation kinetic is not controlled by a single phenomenon. For the highest temperatures (1150–1200 °C), an oxidation rate increase is also observed for long holding durations, followed by an important oxidation rate decrease. This phenomenon could be due to the formation of cracks, providing a diffusion path for oxygen and involving an acceleration of oxidation. But due to oxidation, crack healing then occurs, inducing a decrease in the diffusion rate of oxygen.

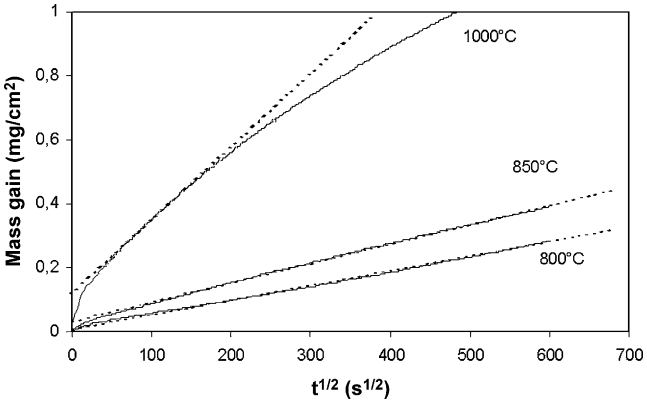

Fig. 6. Comparison between TGA results up to 1000 °C, in continuous line, and parabolic kinetics, in doted line.

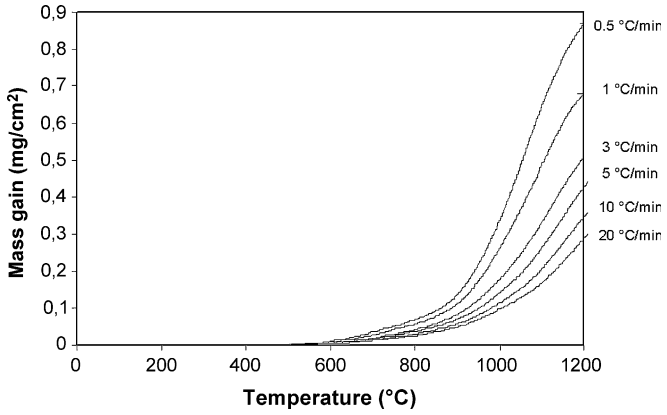

Fig. 7. Results of non-isothermal TGA from 20 to 1200 °C in air of the Si_3N_4–TiN ceramic.

3.3. Non-isothermal TGA curves

Fig. 7 shows the sample mass variations recorded during the non-isothermal oxidation of Kersit 601 between 20 and 1200 °C, for different heating rates ranging from 0.5 to 20 °C/min.

Material oxidation starts from 500 to 550 °C, and remains rather slow up to 800 or 900 °C. The mass gain measured corresponds then to the oxidation of the TiN phase which is transformed in TiO_2 [29]. For higher temperatures, oxidation first accelerates because of the increase of the species mobility (O and Ti) in TiO_2 and TiN phases. Above 1000 °C, oxidation accelerates again because of the oxidation of the silicon nitride phase [4–6]. At about 1100 °C, the curves present an inflection point for the lowest heating rates, which seems to show that the oxidation product formed then is less permeable to the diffusion of the various species than the product formed at lower temperatures. This could be due to the silica formation, which creeps and fills in the sub-layer porosity [29].

4. Phenomenological modeling and oxidation kinetics

Based on these experimental results, and on previous microstructural analysis [29,30], a three-step model is proposed to describe the isothermal oxidation process between 1000 and 1200 °C.

In a first step, the TiN phase is rapidly oxidized to TiO_2. Two mechanisms are in competition for the control of TiN oxidation: titanium and oxygen diffusion through TiO_2. Above 1000 °C, Ti diffusion is faster than oxygen, and TiN oxidation is controlled by titanium diffusion towards the surface [27,28]. The outer diffusion of titanium creates porosity, which decreases the surface area available for diffusion (Fig. 8). The oxidation kinetic of the TiN phase is then characterized by the kinetic parameter $S_{Ti/TiO_2} k p_{Ti/TiO_2}^{1/2}$, where $kp_{Ti/TiO2}$ is the parabolic rate constant corresponding to TiN oxidation by titanium diffusion through TiO_2, and S_{Ti/TiO_2} is the available surface area for titanium diffusion. The surface area S_{Ti/TiO_2} decreases with the growth of porosity in TiN phase, and can be given by Eq. (9) [30]:

$$S_{Ti/TiO_2} = S_{TiN}\left(\frac{1}{at^{1/2}+1}\right) \tag{9}$$

where S_{TiN} is the outer surface of the TiN phase in the as-received material, a is a parameter depending on temperature [30], and t is the time.

Oxidation of the TiN phase then slows down.

At the same time, oxidation of the Si_3N_4 phase occurs, but at a slower rate than TiN during this first step. It is controlled by O diffusion through SiO_2, characterized by the parabolic rate constant $k p_{O/SiO_2}$.

The mass gain per unit area is the addition of the mass gain due to TiN oxidation and to Si_3N_4 oxidation, and can be given, during this step which is considered as a first transient mode, by Eq. (10) [30]:

$$\frac{\Delta m}{S} = \int_0^t \left(\frac{S_{Ti/TiO_2}}{S} k p_{Ti/TiO_2}^{1/2} + \frac{S_{Si_3N_4}}{S} k p_{O/SiO_2}^{1/2}\right) t^{-1/2}\,dt \tag{10}$$

where $S_{Si_3N_4}$ is the outer surface of the Si_3N_4 phase in the as-received material.

Assuming that $S_{Si_3N_4}/S$ and S_{TiN}/S are equivalent to the volume fraction of Si_3N_4 and TiN phases in the material, i.e. 0.7 and 0.3 respectively, then:

$$\frac{\Delta m}{S} = \frac{0.3}{a} k p_{Ti/TiO_2}^{1/2} \ln\left(at^{1/2}+1\right) + 0.7 k p_{O/SiO_2}^{1/2} t^{1/2} + \frac{\Delta m_0}{S} \tag{11}$$

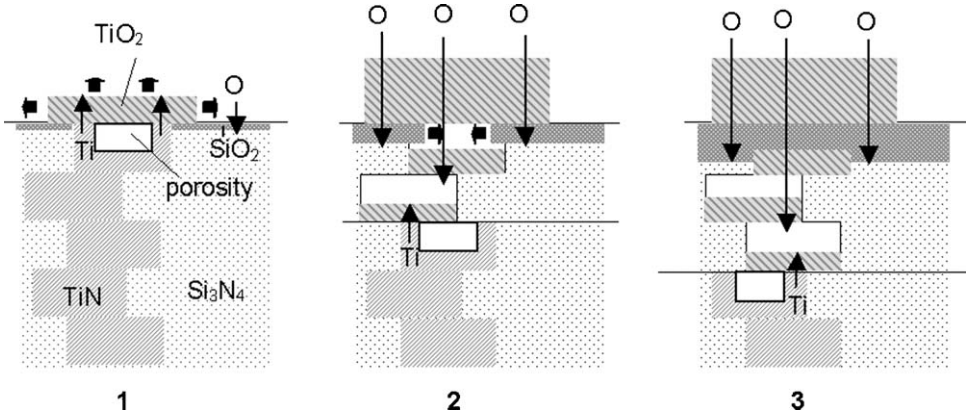

Fig. 8. Schematic description of the three steps of the oxidation model for temperature >1000 °C.

where Δm_0 is a constant corresponding to the mass gain at the beginning of the isothermal dwell.

In a second step, TiN oxidation becomes controlled by O diffusion, which can cross the created porosity in a molecular form. Si_3N_4 oxidation continues and leads to the formation of silica (SiO_2), which has a higher molar volume than Si_3N_4. Silica creeps into the porosity, and progressively overlaps the sub-layer. The surface area S_{SiO_2} of the sub-layer covered by silica is then given by Eq. (12.a) [30]:

$$S_{SiO_2} = S_{Si_3N_4}(1 + bt^{1/2}) \quad (12.a)$$

where b is a parameter depending on temperature.

TiN oxidation is then controlled by two simultaneous mechanisms: O diffusion through TiO_2, and O diffusion through SiO_2 (Fig. 8). The diffusion rate of oxygen in TiO_2, characterized by the parabolic rate constant kp_{O/TiO_2}, being higher than in silica, the creep of SiO_2 in the sub-layer porosity decreases the average oxidation rate of the TiN phase. It is characterized, in this step, by the kinetic parameter $S_{O/TiO_2}kp_{O/TiO_2}^{1/2} + S_{SiO_2/TiO_2}kp_{O/SiO_2}^{1/2}$, where S_{O/TiO_2} corresponds to surface area of TiO_2 phase in the sub-layer not covered by SiO_2, which decreases, and S_{SiO_2/TiO_2} the surface area covered by SiO_2 (Fig. 8). This kinetic parameter also controls the O diffusion rate during the first step, but is then slower than the kinetic parameter of Ti diffusion. The transition time, t_1, between first and second step, corresponds to the equality between the kinetic parameters of the two competitive mechanisms, and is obtained by solving Eq. (13):

$$S_{Ti/TiO_2}(t_1)kp_{Ti/TiO_2}^{1/2} = S_{O/TiO_2}(t_1)kp_{O/TiO_2}^{1/2} + S_{SiO_2/TiO_2}(t_1)kp_{O/SiO_2}^{1/2} \quad (13)$$

The mass gain per unit area, during this second step, called in our model the second transient mode, is given by relation (14):

$$\frac{\Delta m}{S} = (0.3kp_{O/TiO_2}^{1/2} + 0.7kp_{O/SiO_2}^{1/2})t^{1/2} + \frac{0.7}{2}(kp_{O/SiO_2}^{1/2} - kp_{O/TiO_2}^{1/2})bt + \frac{\Delta m_0'}{S} \quad (14)$$

where $\Delta m_0'$ is a constant.

After a time t_2, the sub-layer is overlapped by SiO_2:

$$S_{SiO_2}(t_2) = S_{Si_3N_4}(1 + bt_2^{1/2}) = S \quad (12.b)$$

Oxidation of both TiN and Si_3N_4 phases is then controlled by O diffusion through silica. Oxidation process has then reached a stationary mode (third step), which is governed by a simple parabolic kinetic law:

$$\frac{\Delta m}{S} = kp_{O/SiO_2}^{1/2}t^{1/2} + \frac{\Delta m_0''}{S} \quad (15)$$

where $\Delta m_0''$ is a constant.

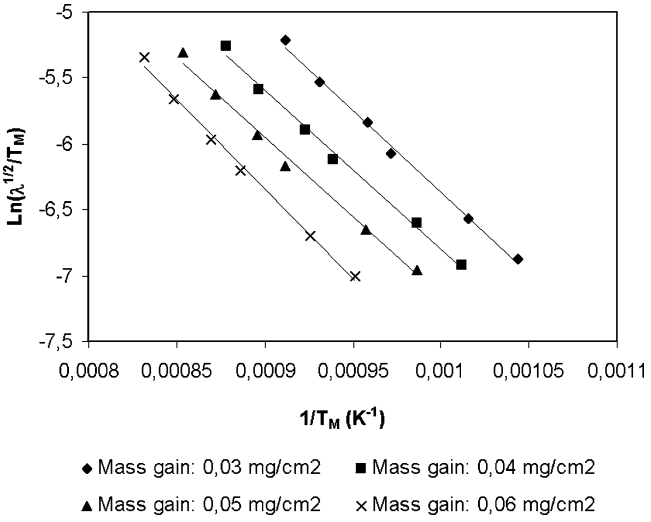

Fig. 9. $\ln(\lambda^{1/2}/T_M) = f(1/T_M)$ curves at constant mass gain deduced from non-isothermal TGA results.

5. Identification of the parameters of the proposed oxidation kinetics

Both non-isothermal and isothermal TGA results were used to identify the various parameters of the kinetic model.

5.1. Non-isothermal TGA investigations

Fig. 9 shows the $\ln(\lambda^{1/2}/T_M) = f(1/T_M)$ experimental curves at a constant mass gain per unit area ($\Delta m/S$), obtained from non-isothermal TGA curves of Figure 7. For low mass gains, experimental points can be fitted by straight lines, which confirms the assumption of a single oxidation mechanism at low temperatures (up to 900 °C). According to Eq. (7), the slope of these straight lines gives the activation energy of this diffusion mechanism.

Fig. 10 shows the activation energy deduced from these curves, versus $\Delta m/S$. After a transitory initial step at low mass gains, activation energy is appreciably constant, up to a mass gain of about 0.06 mg/cm^2. This value corresponds to the validity limit for the non-isothermal analysis described in Section 2.3. For this mass gain value, temperature of non-isothermal TGA curves is between 850 and 900 °C for the highest heating rates (Fig. 7), and a change in oxidation mechanism appears.

This non-isothermal study gives two indications:

- First, the activation energy corresponding to the diffusion mechanism of O through TiO_2 is about 190 kJ mol^{-1} (Fig. 10). This value is in accordance with the results of Lefort et al. [24,27,28], who proposed activation energy between 184 and 196 kJ mol^{-1} for TiN oxidation below 1000 °C. The activation energy of 162 kJ mol^{-1} determined by Bellosi et al. [6] is lower, but appreciably close to the value of the present study.
- Second, the transient temperature, separating TiN oxidation mechanisms controlled by O diffusion and Ti diffusion in

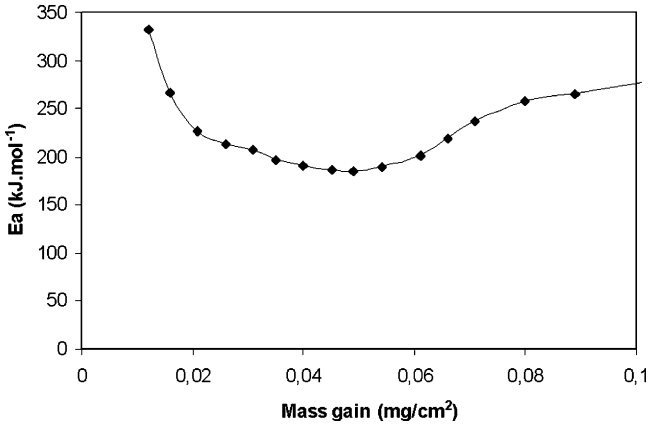

Fig. 10. Activation energy calculated from Fig. 9 for oxygen diffusion through TiO_2 phase.

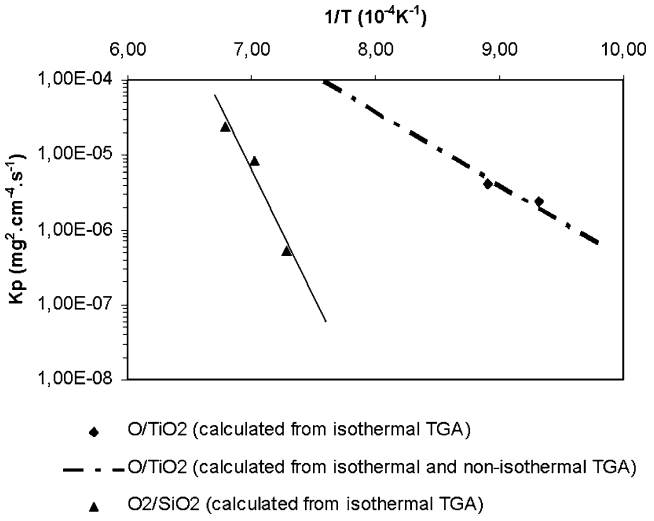

Fig. 11. Evolution of the parabolic rate constants versus temperature for the two main diffusion mechanisms (oxygen diffusion in TiO_2 and in SiO_2) involved in the oxidation process.

TiO_2 is located between 850 and 900 °C. This is in accordance with the data in the literature, which indicates generally a change of diffusion mechanism in TiO_2 at about 900 °C [35].

5.2. Isothermal TGA investigations

At 800 and 850 °C, isothermal oxidation kinetic is parabolic, and TGA curves can be fitted in accordance with relation (8), where the constant K is linked to the parabolic rate constant, $k_{p_{O/TiO_2}}$ characterizing the diffusion rate of oxygen in TiO_2 according to Eq. (16):

$$K = k_{p_{O/TiO_2}} \left(\frac{S_{TiN}}{S}\right)^2 \tag{16}$$

The $k_{p_{O/TiO_2}}$ values obtained according to the two isothermal TGA curves below 900 °C, added to the activation energy value determined in Section 5.1, allow the $k_{p_{O/TiO_2}}$ variation versus temperature (Fig. 11) to be evaluated:

$$k_{p_{O/TiO_2}} = 3.1 \times 10^3 \exp\left(-\frac{22800}{T}\right) \quad (\mathrm{mg^2\,cm^{-4}\,s^{-1}}) \tag{17}$$

Above 1000 °C, Si_3N_4 oxidation becomes faster, and both Si_3N_4 and TiN phases are oxidized simultaneously. According to the oxidation model, for long oxidation duration, the process is controlled only by O diffusion through SiO_2, as for Si_3N_4 oxidation (step 3 of the oxidation model). This indicates that the last part of isothermal TGA curves, above 1000 °C, should be parabolic (Eq. (15)). That is observed at 1100 °C, from about 34 h, but not really at 1150 and 1200 °C (Fig. 5). This phenomenon could be explained by the crystallization of silica at high temperatures, and/or the cracking of the oxide scale, which modifies oxidation kinetic. However, we have considered in the last part of TGA curves at 1100, 1150 and 1200 °C a parabolic range (between the times t_2, where the parabolic mode begins, and t_f, where fluctuations appear) to calculate the parabolic rate constant $k_{p_{O/SiO_2}}$ characterizing oxygen diffusion through silica. Results are given in Table 1 and Fig. 11. Activation energy of O diffusion through SiO_2, calculated from these results, is equal to 644 kJ mol^{-1} (Fig. 11). This value can be compared to bibliographical data for Si_3N_4 oxidation. Bellosi et al. [6] calculated an activation energy of 630 kJ mol^{-1} for a silicon nitride prepared with 3 wt.% Al_2O_3 and 8 wt.% Y_2O_3, a composition close to the matrix phase of Kersit 601. Persson et al. [23], in a study on SiAlON oxidation,

Table 1
Kinetic parameters associated to the parabolic oxidation mode (third step of the oxidation model).

T (°C)	Time range of parabolic mode		$k_{p_{O/SiO_2}}$ ($mg^2\,cm^{-4}\,s^{-1}$)	b (Eq. (12.b))
	t_2[a] (h)	t_f[b] (h)		
1000	3071[e]	–	8.19×10^{-9}[d]	1.29×10^{-4}
1100	34[c]	108[c]	5.29×10^{-7}[c]	1.22×10^{-3}
1150	4.7[c]	49[c]	8.58×10^{-6}[c]	3.35×10^{-3}
1200	0.7[c]	13.4[c]	2.38×10^{-5}[c]	8.57×10^{-3}

[a] t_2 is the oxidation time at the beginning of the parabolic mode.
[b] t_f is the oxidation time corresponding to the beginning of oxidation rate fluctuations.
[c] According to TGA curves.
[d] According to Eq. (17).
[e] According to Eq. (18).

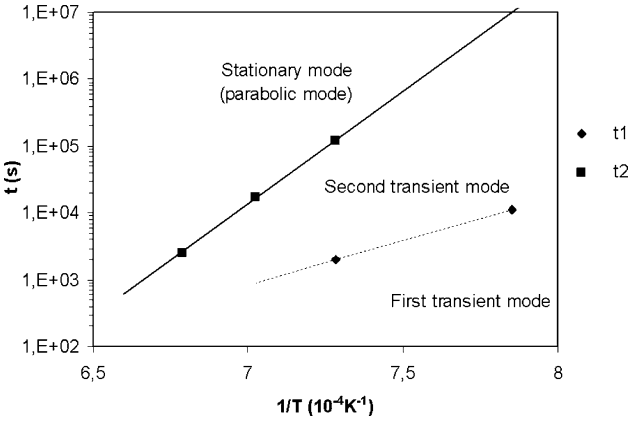

Fig. 12. Evolution of the time t_1 separating the first and second transient modes, and of the time t_2 separating the second transient mode and the stationary mode.

calculated an activation energy of 710 kJ mol^{-1}, for a material containing 6 wt.% Y_2O_3. The activation energy value calculated in the present study is then in accordance with the data in the literature.

The beginning of the parabolic mode corresponds to a quantity of formed silica sufficient to overlap the whole material surface. Assuming that this quantity is not temperature-dependent, and considering that SiO_2 formation is diffusion-controlled, the time t_2 corresponding to the beginning of the parabolic mode depends on the temperature according to Eq. (18):

$$t_2 = C \exp\left(\frac{E_{a_2}}{RT}\right) \tag{18}$$

where C is a constant, and E_{a_2} is the activation energy associated to O diffusion through SiO_2.

Fig. 12 shows the t_2 values versus $1/T$, determined from TGA curves (Table 1). These points follow appreciably a linear variation, and the deduced activation energy is equal to 655 kJ mol^{-1}. This value is very close to the activation energy obtained from Fig. 11 (644 kJ mol^{-1}), which confirms the validity of our considerations.

According to these results, the parabolic rate constant of Si_3N_4 oxidation (characterizing O diffusion through silica) is

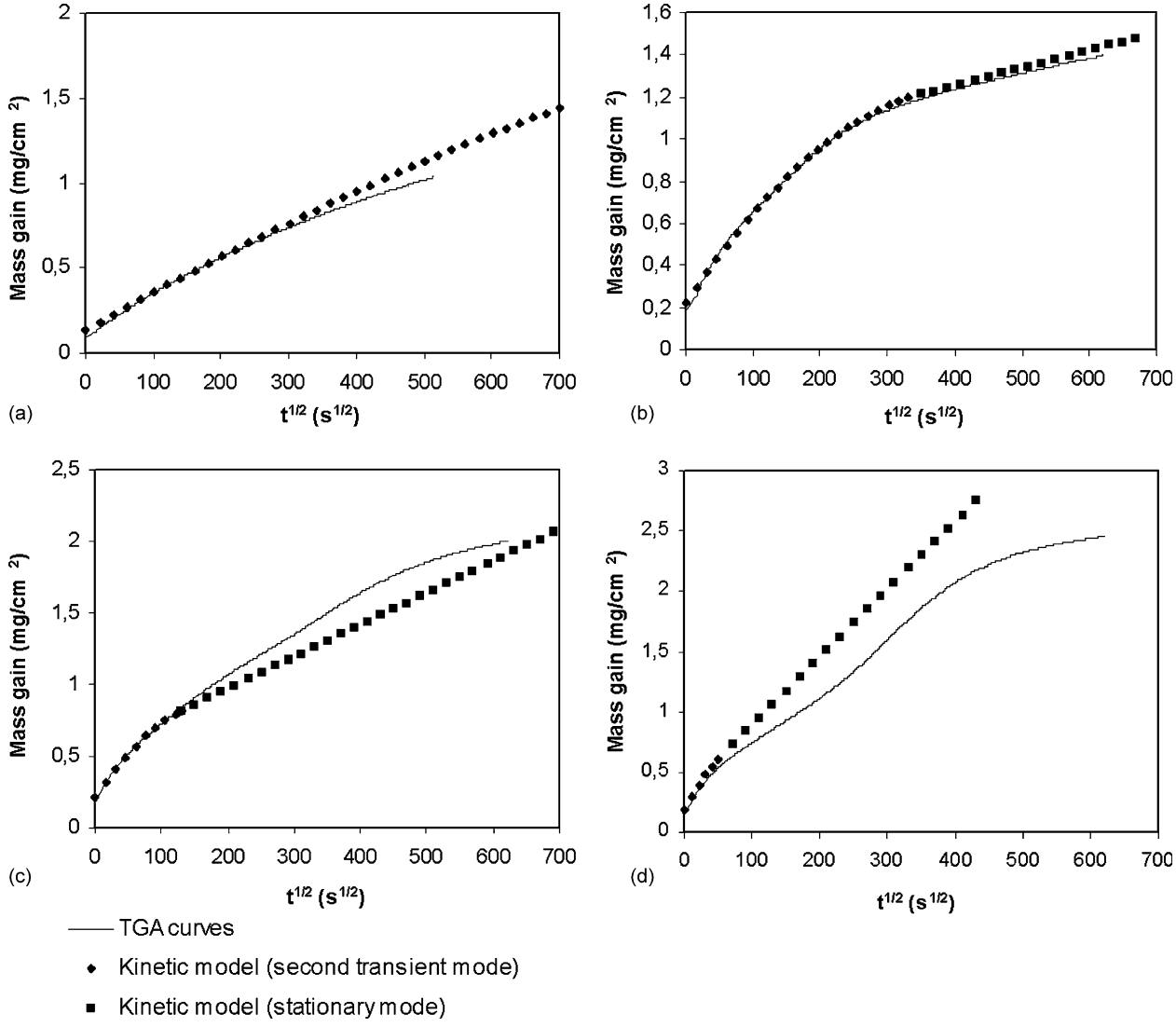

Fig. 13. Comparison between the kinetic model and the TGA curves at 1000 °C (a), 1100 °C (b), 1150 °C (c) and 1200 °C (d).

given by relation (19):

$$k p_{O/SiO_2} = 2.09 \times 10^{18} \exp\left(-\frac{77400}{T}\right) \quad (mg^2\,cm^{-4}\,s^{-1}) \tag{19}$$

6. Comparison between kinetic model and TGA investigations above 1000 °C

The first transient mode (Ti diffusion towards the surface) is very fast, especially at high temperature. The first mode being considered negligible, the theoretical oxidation kinetics (Eqs. (14) and (15)) can be plotted using data obtained in previous sections (Eqs. (17)–(19)). The b parameter is calculated from Eq. (12.b), using t_2 values determined from equation 18 and TGA curves (Table 1). Comparison between theoretical kinetics and experimental curves are given in Fig. 13. During the second transient mode (second step of the model), calculated curves are overall in accordance with the experiment. The stationary mode (parabolic mode, i.e. third step of the model) is not reached on TGA curve at 1000 °C after 108 oxidation hours (Fig. 13a). This is in accordance with theoretical kinetics, which predicts the beginning of stationary mode at 1000 °C after about 3000 oxidation hours (Eq. (18), Table 1).

At 1100 °C, stationary mode is reached after 34 oxidation hours according to the TGA curve (Fig. 13b), and theoretical kinetic is in accordance with the experiment. At 1150 and 1200 °C, on the other hand, parabolic mode is not exactly observed (Fig. 13c, d). TGA curves present fluctuations, especially at 1200 °C, with successive increase and decrease in oxidation rate. The phenomenon can be related to the crystallization of silica, which has already been observed [18,23]. This process has two contrasting effects:

- the crystallization of silica decreases the diffusion rate of oxygen through compact SiO_2;
- this transformation can create cracks, which increase oxidation rate.

The TGA-curve aspect at 1150 and 1200 °C can then be explained by a succession of cracking of oxide scale (oxidation rate increases), and crack healing (oxidation rate decreases). Then, when this phenomenon is observed, parabolic kinetic is not convenient, which explains the gap between experimental and modeled curves.

The beginning of TGA curves at 1000 and 1100 °C are not perfectly fitted by the kinetic model corresponding to the second transient mode. This could be due to the fact that the first transient mode (TiN oxidation controlled by Ti diffusion through TiO_2), which is longer for the lowest temperatures, has been neglected. According to our model, this first transient mode can be modeled by Eq. (11). The $k p_{Ti/TiO_2}$ parameter, which has not been determined in this study, can be evaluated from bibliographic data. Kofstadt proposed an activation energy for Ti diffusion through TiO_2 of about 270 kJ mol^{-1} [35]. Assuming that the temperature of mechanism change for the TiN oxidation is 900 °C (that means at 900 °C $k p_{Ti/TiO_2} = k p_{O/TiO_2}$), we can propose the following relation for the $k p_{Ti/TiO_2}$ variation:

$$k p_{Ti/TiO_2} = 1.29 \times 10^{7} \exp\left(-\frac{32500}{T}\right) \quad (mg^2\,cm^{-4}\,s^{-1}) \tag{20}$$

The parameter of Eq. (11) can be calculated from the time value, t_1, corresponding to the beginning of the second transient mode using Eq. (13).

Table 2 gives the t_1 values and a parameters determined according to isothermal TGA curves and Eq. (13). Fig. 14 shows the comparison between the kinetic model, with both transient modes, and experimental TGA curves at 1000 and 1100 °C. The kinetic model corresponding to the first transient mode can be observed to give a better fitting of the beginning of TGA curves than the kinetic law corresponding to the second transient mode.

Table 2
Kinetic parameters associated to the first oxidation mode.

T (°C)	t_1[a] (s)	a[b]
1000	13,000	3.87×10^{-3}
1100	2,025	2.42×10^{-2}

[a] Estimated according to Fig. 13a, b.
[b] Calculated from Eq. (13).

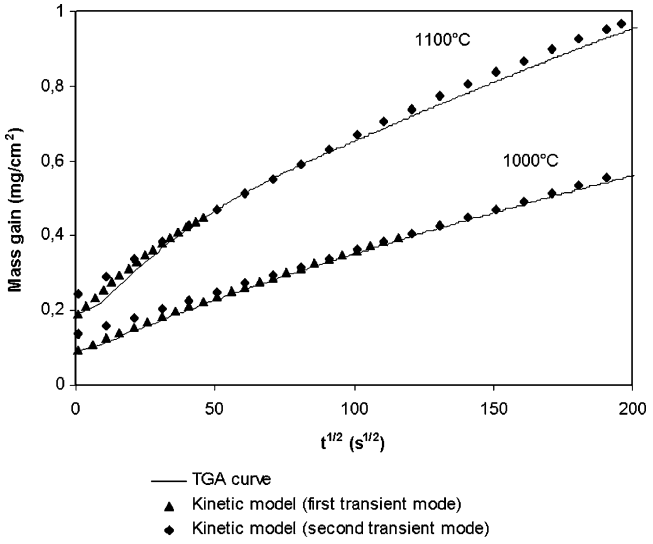

Fig. 14. Comparison between the kinetic model and the TGA curves at the beginning of the isothermal oxidation (transient modes).

7. Conclusion

Based on a phenomenological approach and on TGA results, a kinetic model for oxidation of a Si_3N_4–TiN composite in the 1000–1200 °C temperature range has been proposed. This model consists in three steps, controlled by different diffusional mechanisms.

In a first step, oxidation of the TiN phase is controlled by titanium diffusion, whereas oxidation of the Si_3N_4 phase is

controlled by O diffusion through SiO_2. The outer diffusion of Ti creates porosity in the sub-layer, which slows down the titanium migration.

During a second step, oxidation of TiN becomes controlled by O diffusion through TiO_2 and porosity, towards inner TiN particles. Si_3N_4 oxidation leads to the formation of vitreous SiO_2, which progressively fills in the sub-layer porosity, forming a continuous layer.

The third step is a parabolic mode, controlled by O diffusion through the continuous SiO_2 sub-layer, which is slower than through TiO_2.

The parameters of the kinetic model suggested for each of the three steps were identified using isothermal and non-isothermal TGA results. The kinetic model compared rather well with the isothermal TGA curves for the two first steps, while for the third step, a gap is observed between kinetic model and TGA curves, above 1150 °C. This phenomenon has been related to the crystallization of the silica phase, which modifies appreciably the oxidation kinetic.

The results presented in this paper confirm the validity of the kinetic model proposed in a previous article [30]. Nevertheless, the maximal temperature of validity for the model must be reduced for longer oxidation duration, because of crystallization of silica at high temperature. This phenomenon could be taken into account by modifying the kinetic laws, as proposed by Persson et al. [23] for Si_3N_4 materials. However, these kinetic models are not suitable when cracking occurs, which is often observed at higher temperatures.

Acknowledgement

We would like to express our gratitude to Mrs. N. Marshall for editing this manuscript.

References

[1] M. Higuchi, M. Miyake, H. Kakeuchi, E. Kamjo, US Patent 8 4 659 508, 1987.
[2] C. Martin, P. Mathieu, B. Cales, Electrical discharge machinable ceramic composites, in: R.J. Brook (Ed.), Proceedings of Symposium on Ceramic Materials Research, E-MRS Spring Conference, Strasbourg (France), 1988.
[3] A. Bellosi, S. Guicciardi, A. Tampieri, Development and characterization of electroconductive Si_3N_4–TiN composites, J. Eur. Ceram. Soc. 9 (1992) 83–93.
[4] Y.G. Gogotsi, F. Porz, The Oxidation of particulate-reinforced Si_3N_4–TiN composites, Corros. Sci. 33 (4) (1992) 627–640.
[5] Y.G. Gogotsi, F. Porz, G. Dransfield, Oxidation behavior of monolithic TiN and TiN dispersed in ceramic matrices, Oxid. Met. 39 (1/2) (1993) 69–91.
[6] A. Bellosi, A. Tampieri, Y.Z. Liu, Oxidation behaviour of electroconductive Si_3N_4–TiN composites, Mater. Sci. Eng. A127 (1990) 115–122.
[7] F. Peni, J. Crampon, R. Duclos, On the morphology and composition of the oxidized layer in Si_3N_4-based materials, Mater. Sci. Eng. A163 (1993) 5–7.
[8] L.U.J.T. Ogbuji, S.R. Bryan, The SiO_2–Si_3N_4 interface. Part I. Nature of the interface, J. Am. Ceram. Soc. 78 (5) (1995) 1272–1278.
[9] L.U.J.T. Ogbuji, The SiO_2–Si_3N_4 interface. Part II. O_2 permeation and oxidation reaction, J. Am. Ceram. Soc. 78 (5) (1995) 1279–1284.
[10] B.W. Sheldon, Silicon nitride oxidation based on oxinitride interlayers with graded stoichiometry, J. Am. Ceram. Soc. 79 (11) (1996) 2993–2996.
[11] D.J. Choi, D.B. Fischbach, W.D. Scott, Oxidation of chemically-vapor deposited silicon nitride and single-crystal silicon, J. Am. Ceram. Soc. 72 (7) (1989) 1118–1123.
[12] H. Du, R.E. Tressler, K.E. Spear, C.G. Pantano, Oxidation studies of crystalline CVD silicon nitride, J. Electrochem. Soc. 136 (5) (1989) 1527–1536.
[13] H. Du, R.E. Tresseler, K.E. Spear, Thermodynamics of the Si–N–O system and kinetic modeling of oxidation of Si_3N_4, J. Electrochem. Soc. 136 (11) (1989) 3210–3215.
[14] H. Du, R.E. Tresseler, K.E. Spear, M. Wang, Annealing studies of coupled Si_3N_4 and SiO_2 films, J. Mater. Sci. Lett. 8 (1989) 1341–1343.
[15] K.L. Luthra, A mixed interface reaction/diffusion control model for oxidation of Si_3N_4, J. Electrochem. Soc. 138 (10) (1991) 3001–3007.
[16] D.P. Butt, D. Albert, T.N. Taylor, Kinetics of thermal oxidation of silicon nitride powders, J. Am. Ceram. Soc. 79 (11) (1996) 2809–2814.
[17] L.U.J.T. Ogbuji, J.L. Smialek, Evidence from transmission electron microscopy for an oxinitride layer in oxidized Si_3N_4, J. Electrochem. Soc. 138 (10) (1991) L51–L53.
[18] M.H. Lewis, P. Barnard, Oxidation mechanism in Si–Al–O–N ceramics, J. Mater. Sci. 15 (1980) 443–448.
[19] L. Wang, C. He, J.G. Wu, Oxidation of sintered silicon nitride materials, in: Proceedings of the third International Symposium on Ceramic Materials and Components for Engines, American Ceramic Society, Las Vegas, (1988), pp. 604–611.
[20] D.R. Clarke, F.F. Lange, Oxidation of Si_3N_4 alloys: relation to phase equilibria in the system Si_3N_4–SiO_2–MgO, J. Am. Ceram. Soc. 63 (9–10) (1980) 586–593.
[21] G. Ziegler, J. Heinrich, G. Wötting, Review: relationships between processing, microstructure and properties of dense and reaction-bonded silicon nitride, J. Mater. Sci. 22 (1987) 3041–3086.
[22] C.O. Meara, J. Sjoberg, Transmission electron microscopy investigation of the oxidation of hot isostatically pressed silicon nitride with and without sintering aids, J. Am. Ceram. Soc. 80 (6) (1997) 1491–1500.
[23] J. Persson, M. Nygren, The oxidation kinetics of β-sialon ceramics, J. Euro. Ceram. Soc. 13 (1994) 467–484.
[24] J. Desmaison, P. Lefort, M. Billy, Oxidation mechanism of titanium nitride in oxygen, Oxid. Met. 13 (6) (1979) 505–517.
[25] A. Tampieri, E. Landi, A. Bellosi, The oxidation behaviour of monolithic TiN ceramic, Br. Ceram. Trans. J. 90 (1991) 194–196.
[26] H. Ichimura, A. Kawana, High-temperature oxidation of ion-implanted TiN and TiAlN films, J. Mater. Res. 8 (5) (1993) 1093–1100.
[27] P. Lefort, J. Desmaison, M. Billy, Oxydation du nitrure de titane par l'oxygène: comportement du nitrure $TiN_{0.95}$ pulvérulent, C. R. Acad. Sci. C 285 (3) (1977) 361–369.
[28] P. Lefort, J. Desmaison, M. Billy, Cinétique d'oxydation du nitrure de titane: comportement de plaquettes de nitrure $TiN_{0,91}$ en atmosphère d'oxygène, J. Less-Common Met. 60 (1978) 11–24.
[29] F. Deschaux-Beaume, N. Fréty, T. Cutard, C. Levaillant, Oxidation of a Si_3N_4–TiN composite: microstructural investigation and modeling, J. Am. Ceram. Soc. 85 (7) (2002) 1860–1866.
[30] F. Deschaux-Beaume, N. Fréty, T. Cutard, C. Colin, Oxidation modeling of a Si_3N_4–TiN ceramic: microstructure and kinetic laws, Ceram. Int. 33 (2007) 1331–1339.
[31] P. Maynier, P.F. Martin, P. Bastien, J. Sebille, Etablissement d'une équivalence entre le temps et la température d'austénitisation—application aux traitements thermiques et au soudage, Rev. Métallurg. LXIII (12) (1966) 997–1012.
[32] M. Toitot, P. Dor, Etablissement d'effet du temps et de la température sur les phénomènes de diffusion: formule paramétrique applicable aux cycles thermiques—détermination des temps de maintien équivalents, Rev. Métallurg. LXIII (12) (1966) 1013–1016.
[33] D. Tiberghien, Caractérisation de l'interface fibre-matrice dans les composites Al/In601 oxydés, Etude de l'influence de l'oxydation des fibres sur les propriétés des composites, Mémoire de l'Université Catholique de Louvain, 1997.
[34] F.X. Gustin, Durcissement structural d'un composite à matrice d'alliage d'aluminium A-S9G03, renforcée par des fibres passivées d'Inox 316L, Mémoire de l'Université Catholique de Louvain, 1998.
[35] P. Kofstad, High Temperature Corrosion, Elsevier Applied Science Publishers Ltd, 1988, pp. 289–298.